THE JOURNAL OF PHYSICAL CHEMISTRY C

Article

pubs.acs.org/JPCC

Electron-Deficient Pyrimidine Adopted in Porphyrin Sensitizers: A Theoretical Interpretation of π-Spacers Leading to Highly Efficient Photo-to-Electric Conversion Performances in Dye-Sensitized Solar Cells

Meiyuan Guo, Rongxing He,* Yulan Dai, Wei Shen, and Ming Li

College of Chemistry and Chemical Engineering, Southwest University, Chongqing 400715, China

Chaoyuan Zhu and Sheng Hsien Lin

Department of Applied Chemistry, Institute of Molecular Science and Center for Interdisciplinary Molecular Science, National Chiao-Tung University, Hsinchu 300, Taiwan

Supporting Information

ABSTRACT: A mass of porphyrin sensitizers have been designed and synthesized for dye-sensitized solar cells in previous works, and almost all of them incorporated an electron-rich system as the π-spacer. We here adopted the electron-deficient pyrimidine as an effective π-spacer and combined a cyanoacrylic acid anchoring group, as such a design yields a more bathochromic shift of the spectral absorption of the dye and results in an improved spectral overlap with the solar spectrum and an enhanced light-harvesting efficiency. The result does tally with the performance of sensitizer adsorbing on a semiconductor. From the electron density difference plots of electron transitions, we found that not all electron transitions could make for the effective electron transfer from donor to acceptor groups, which means the sensitizer performance in dye-sensitized solar cells not only relies on the extrinsic spectral absorption intensity but also depends on the intrinsic character of electron movement related to electron excitation. Moreover, the introduction of electron-deficient pyrimidine could affect the energy levels of excited molecules in solution, further affecting the kinds of electron transfer processes. We presented several novel porphyrin sensitizers for comparison on how the π-spacer and anchoring group influence the optical absorption, electron transfer processes, and regeneration of the oxidized dyes, thereby gaining potential dye-sensitized solar cells with highly efficient photo-to-electric conversion performances.

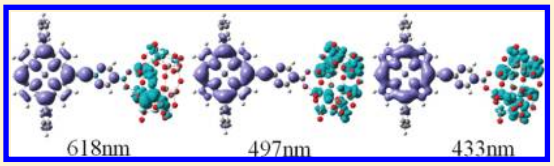

1. INTRODUCTION

With the exhausting of natural resources and the increasing demand for environmentally friendly energy, more and more attention has been paid to the development of alternative energy resources.[1] Among various renewable energy resources, solar energy is the most viable to meet our energy requirement.[2] Since 1991, lots of investigations were made on the synthesis and characterization of various sensitizers after O'Regan and Grätzel reported an efficient performance of dye-sensitized solar cells (DSSCs) based on the ruthenium complexes.[3] In nanocrystalline TiO_2-based DSSCs, a photo-to-electric conversion efficiency of up to 11% had been obtained using ruthenium dyes.[4] However, the drawback of ruthenium complexes is the limited absorption in the near-infrared region (NIR) of the solar spectrum. The limited availability of these Ru dyes together with their undesirable environmental impacts have led to the search for more excellent and safer dyes. At present there is a strong interest in developing promising photosensitizers that have the advantage of high extinction coefficients and can thus also meet the demand of good light-harvesting efficiency with thinner TiO_2 films.[5] Furthermore, as one of the vital parts of DSSCs, the sensitizer should have a suitable anchoring group to bind the dye onto the semiconductor surface, proper redox potentials to match the semiconductor, and electrolyte for effective electron injection and regeneration of the oxidized dyes, respectively.[6] The porphyrin system exhibits intense spectral response bands in the visible region and even the part of the near-infrared region, possesses good chemical, optical, and thermal stabilities, and provides good potential candidates for photovoltaic applications. Kay and Grätzel in their pioneering work on porphyrin dye reported a photo-to-electric conversion efficiency value of 2.6%.[7a] So far, the reported most efficient porphyrin dye, which attained a photo-to-electric conversion efficiency value of 7.47%, is comparable to the performance of ruthenium-based dyes, such as N3 dye (*cis*-bis(4,4′- dicarboxy-2,2′-bipyridine) dithiocyanato ruthenium(II); the photo-to-electric conversion efficiency value is 7.68%).[7b] The boosted performance offered a good prospect for porphyrin dyes as photosensitizers in the DSSCs.

Received: November 15, 2011
Revised: March 24, 2012
Published: March 24, 2012

dx.doi.org/10.1021/jp2109829 | J. Phys. Chem. C 2012, 116, 9166–9179

In search of promising porphyrin sensitizers, a large number of porphyrin derivatives have been synthesized, and their photochemical properties have been analyzed.[8] The porphyrin system exhibits intense and wide optical absorption stems from their appropriate highest occupied molecular orbital (HOMO) and lowest occupied molecular orbital (LUMO) energy levels and achieves strong absorption in the 350−500 nm and 550−700 nm regions, which are assigned to the *B* (or Soret) band and *Q* band, respectively. These porphyrin derivatives can be suited as panchromatic photosensitizes for DSSCs. Besides, several studies have also demonstrated that porphyrin dyes can show efficient photoinduced electron injection into the conduction band of TiO_2.[8a,9]

Bignozzi and co-workers[10a] studied the effects of different anchoring groups (phosphoric acid and carboxylic acid anchoring groups) and substitution positions on DSSC performance by constructing a series of porphyrin sensitizers. They concluded that the electronic coupling between sensitizer and semiconductor is one of the key parameters in the design of efficient DSSCs. In addition, they demonstrated that the differences in the orientation and distance of the chromospheres on the crystal surface imposed by the directionality of the anchoring groups could result in different incident photon to current conversion efficiency (IPCE) values.

Nazeeruddin and co-workers[10b] studied a series of porphyrin sensitizers with different central metal ions and found that the IPCE values of diamagnetic metalloporphyrins containing Zn with carboxylic anchoring group are much higher than that of paramagnetic metalloporphyrins containing Cu. Furthermore, they showed that porphyrins with a carboxylate anchoring group have higher efficiencies than those with a phosphonate anchoring group. Imahori and co-workers[11] paid much attention to the effects of different π-spacer systems (such as the thienyl and furyl π-spacers substituted at the β-position of porphyrins) on the performance of DSSCs, and their results indicated that different π-spacers would lead to very different performance of DSSCs, owing to variation of adsorption behaviors.

Many works also have been put into the question of how the donor−acceptor (D−A) distances and donor−bridge energy gaps affect the electronic coupling and thus the rates of electron injection. Kim and co-workers[12] investigated electronic and photovoltaic properties of functionalized porphyrins at *meso*-positions and β-positions with different carboxylic acid groups in DSSCs. They claimed that the effective electronic coupling through the bridge plays an important role in the electron injection process. The longer distance between the dyes and the TiO_2 surface exhibited better performance due to a slower charge recombination rate. While Diau and co-workers[13a] developed a family of porphyrin derivatives with varied length bridges to facilitate the electron transport, the efficiency of these devices decreased systematically with increasing length of the linker, although the rates of electron injection between dyes and TiO_2 were equal. Recently, several new porphyrin dyes with the typical D-π-A structure have been reported by Tan and co-workers:[13b] the porphyrin moiety acted as an electron donor group, and cyanoacrylic acid was used as an anchoring group; different thiophene derivatives, known as an electron-rich system, acted as a π-bridge to improve spectral absorption. They found that the thiophene π-conjugation unit can extend the spectral overlap region of porphyrin dyes.

From these works performed by predecessors, we found that practically all porphyrin dyes incorporate electron-rich systems as the π-spacers, for instance, thiophene derivatives,[11,13b] furyl,[11] and phenyl.[13a,c,d] However, such a design only yields a limited bathochromic shift in spectral absorption and limited performance in DSSCs. A few organic D-π-A dyes that incorporated electron-deficient heteroarenes such as quinoline,[14a] isoxazole,[14b] and thiazole[14c] moieties as linkages to cyanoacrylic acid showed an improved spectral overlap with the solar spectrum and enhanced the light-harvesting efficiency. However, the absence of effective charge separation inhibited their performance in DSSCs. Questions may be raised on what is the effect of the π-spacer intrinsic character on the performance of DSSCs? How do the electron-deficient and rich-electron π-spacers affect the charge separation in the donor−bridge−acceptor system? We here introduce an electron-deficient pyrimidine as the π-spacer combined cyanoacrylic acid anchoring group as a model for parallel comparison with the porphyrin-bridged phenylene and carboxylic acid anchoring group. The purpose of this design is to consider the effects of π-spacers with electron-deficient and rich-electron groups on the charge separation in D-π-A systems and the performance of DSSCs. As a result, the HOMO−LUMO energy gap is decreased in this case. This change is reflected in the remarkable bathochromic shift and broadening of the absorption spectra and hence improving the light-harvesting range. To our best knowledge, it is the first time that the electron-deficient pyrimidine is used as the π-spacer of porphyrin photosensitizers to investigate theoretically the performance of DSSCs. By comparing the experimental observations, our calculation results indicated that the new systems should have better performance due to their wider optical absorption, especially the better driving force, more outstanding charge separation, and more favorable regeneration of the oxidized dye. We also found that the strong spectral absorption does not always promote the effectual electron separations, which means that the performances of the sensitizers not only rely on the extrinsic spectral absorption intensity but also depend on the intrinsic character of the electron transition. More detailed discussions about how the electron-deficient π-spacer and cyanoacrylic acid improve the performance of photosensitizers in the DSSCs were presented in the text. In our simulation, the DSSC was structured as the typical cell described widely elsewhere, in which the semiconductor is TiO_2 with a valence band (VB) and conductive band (CB) of 2.76 and −0.44 V, respectively.[6,15] The iodine/triiodide couple is used as a regenerator of the DSSCs, and the redox potential of the iodide/triiodide electrolyte is about +0.30 V relative to the normal hydrogen electrode (NHE).[6]

2. COMPUTATIONAL METHODS

Nowadays, molecular modeling techniques and especially quantum chemistry offer a competitive alternative for the interpretation of experimental data and even offer predictability of novel materials arising from industrial interests and developments. The improvements in computer technology now allow the study, at correlated levels of approximation, of the properties of large molecular species such as the DSSC dyes and crystal cluster.

In the present work, full geometry optimizations and electronic structure calculations of porphyrin sensitizers were first performed in vacuum using the B3LYP functional with 6-31G(d) basis set.[16a] To obtain relatively accurate energies and compare with the available experimental results, the ground-state geometries of the studied porphyrin sensitizers in solvent

dx.doi.org/10.1021/jp2109829 | J. Phys. Chem. C 2012, 116, 9166−9179

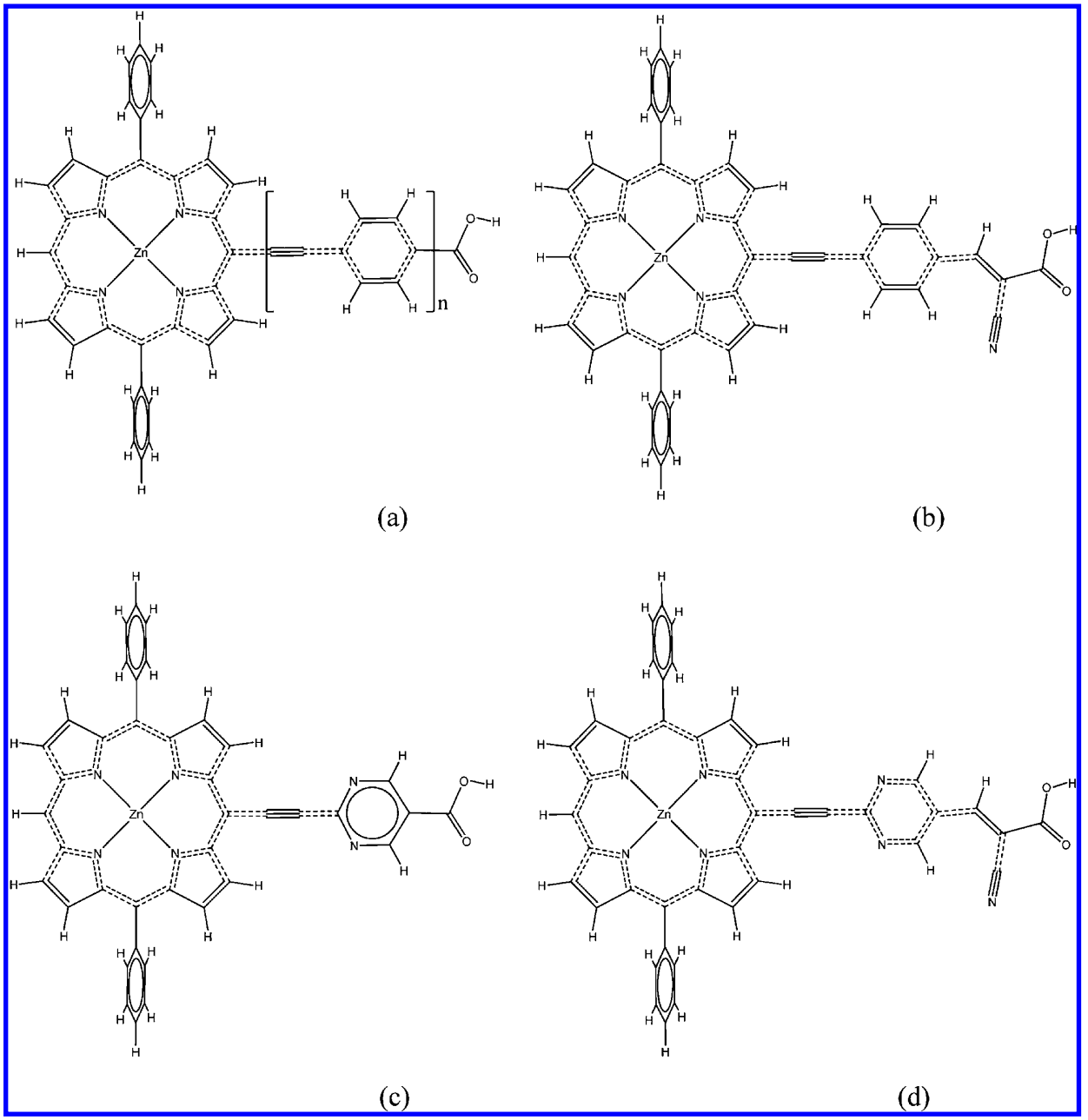

Figure 1. Molecule structures of porphyrin sensitizers: (a) ZnBPP-PE$_n$ (n = 1, 2, 3), (b) ZnBPP-PECN, (c) ZnBPP-PMC1, and (d) ZnBPP-PMCN.

tetrahydrofuran (THF) were reoptimized by using the polarized continuum model (PCM) with larger basis set 6-311G(d,p). Frequency calculations at the same level were performed to confirm each stationary point to be a true energy minimum. For the purpose of investigation of the DSSC properties, the geometry optimizations of the system comprising porphyrin sensitizers and a $Ti_{16}O_{32}$ model were performed using the B3LYP/6-311G(d,p) level, in which the used basis set for Ti atoms was the standard LANL2DZ. The densities of states (DOS) and projected densities of states (PDOS) for the optimized surface complex structures were investigated. The results described clearly the composition of the upper valence band and lower conductive band regions. For the sake of evaluating the overall coupling interaction between sensitizer and TiO_2 cluster, the calculation of the properties of the selected molecular orbitals was carried out. The lowest singlet excited-state geometries of porphyrin sensitizers were computed with time-dependent density functional theory (TD-DFT)[16b−d] on the basis of the optimized ground-state geometries. To calculate the redox potentials, the geometries of the oxidized porphyrin sensitizers in solvent THF were also optimized using the B3LYP/6-311G(d,p) level. All redox potentials involved in this study were obtained versus the NHE. The electronic absorption spectra of sensitizers and the surface complexes were calculated with the TD-DFT method. Furthermore, the electron density differences were calculated and compared for screening of the sensitizer candidates for DSSCs with effective charge separation. The electron densities of all orbitals that related to the electron transitions were calculated with code Multwfn 2.1.[17]

It is well-known that for charge-transfer transitions TD-DFT should underestimate the excitation energies. In addition, the argument whether or not DFT orbital energy has clear physical meaning is still existing. Therefore, in the present work the HF

dx.doi.org/10.1021/jp2109829 | J. Phys. Chem. C 2012, 116, 9166−9179

and CIS methods were used to reestimate all the results from DFT and TD-DFT calculations. The obtained geometries, electron density differences, and excitation energies (see Supporting Information) agree well with the DFT and TD-DFT results and the available experimental data. Generally, DFT and TD-DFT can provide an improved treatment of the electron correlation effects relative to HF and CIS and, as a result, show better agreement with the experimental spectra. The TD-DFT approach is similar to CIS in implementation[18a] but is different in concept. Kohn–Sham molecular orbitals (MOs) of DFT are used to represent the one-electron density, while HF orbitals have well-defined chemical interpretations: frontier orbitals are used to describe chemical reactivity, and orbital energies are related to excitation energies via Koopman's theorem. The simple HF ground state Hamiltonian used in CIS is replaced in TD-DFT by sophisticated DFT functionals that take electron correlation into account. As extensively discussed in Rosa's work,[18b] the Kohn–Sham orbital model is very suitable for interpretation of the electronic structure and elucidation of the character of the excitations. They are thus used routinely to provide a useful tool for qualitative analysis of chemical properties.[18c] The electronic structures of ruthenium dyes,[19a−c] TiO_2 solids,[19d] and nanocrystal[19e] as well as dye-sensitized TiO_2[19f] have all been successfully analyzed in this way. We are therefore confident that the presented analysis based on the Kohn–Sham orbitals is useful for an improved understanding of the electronic structure of the studied systems.

These above-mentioned calculations were used to achieve insights into the geometrical and electronic structures of the dyes and to bring up the adequate structural modifications to optimize the properties of the porphyrin-based DSSCs. All DFT, HF, CIS, and TD-DFT calculations were performed using the Gaussian 09 program.[20]

3. RESULTS AND DISCUSSION

On the basis of the previous experimental results,[8−14] in the present work we investigated the influence of electron-deficient and electron-rich groups as the π-spacer on electron transition in the push–pull DSSC system, and the effects of the anchoring groups on the electron transition were also included. These studies helped us to find out the relationship between the molecular electronic structure of the porphyrin sensitizer and the performance of the porphyrin-sensitized solar cells and brought to light how the photophysical properties play a key role in DSSC efficiency. The property analysis of a series of novel zinc porphyrins with 1−3 π-conjugated phenylethylnyl (PE) units (labeled PE1–PE3) as a link of controlled length synthesized by Diau and co-workers[13a] was implemented first, and the results obtained by means of our analytic method nicely reproduced the experimental evidence (detailed theoretical results were presented in the Supporting Information). Further, we explained why the best photo-to-electric conversion efficiency in this series of porphyrin sensitizers is only 2.7%, which urged us to improve the performance by modifying the electronic structure of the porphyrin sensitizer. After that, we designed several novel promising photosensitizes and predicted their properties in comparison with the experimental data of sensitizers in Diau's work.[13a] Our investigation proved that the electron-deficient pyrimidine system should be an effective π-spacer for highly efficient DSSCs, and the cyanoacrylic acid should be more suitable as an anchoring group for porphyrin sensitizer systems.

3.1. Geometries of Ground States. A large number of works have been performed to meliorate the zinc–porphyrin structure and design more efficient DSSCs.[11,13a,c,21] Kinds of functional electron donor groups have been adopted on the zinc-porphyrin periphery, which could improve the red-shift absorption spectrum due to the decrease of the optical energy gap. Further, modifying the *meso*-position or the β-position of metalloporphyrins with varied π-conjugated groups could extend the π-systems and obtain more bathochromic Q bands as a result of splitting of the frontier molecular orbitals. This indicates that the intrinsic character of the extended π-spacer is vital to a promising photosensitizer. In the present work, 10,20-biphenylporphinato zinc(II) (ZnBPP) is served as a light-harvesting center (Figure 1), which possesses a stability against irradiation and the facilities to synthesize and improve chemical structures (hence their electrochemical and photochemical properties). The $Ti_{16}O_{32}$ cluster, the small nanocrystal model reported in Persson's work,[21a] was used as the electron acceptor in our DSSC model. ZnBPP and its derivatives with varied length phenylethylnyl (PE) units connecting carboxylic acid were synthesized by Diau and coworkers, and the efficiencies of these devices decreased systematically with the increasing length of the linker. The best efficiency was obtained by 5-(4-carboxy-phenylethynyl)-10,20-biphenylporphinato zinc(II) (denoted as ZnBPP-PE1). In our work, three novel porphyrin sensitizers were designed, and the detailed comparisons in properties between novel porphyrin dyes and ZnBPP-PE1 were carried out. These novel dyes are 5-(4-cyanoacry-pyrimidiny-lethlnyl)-10,20-biphenylporphinato zinc(II) (denoted as ZnBPP-PMCN), 5-(4-cyanoacry-phenylethynyl)-10,20-biphenyl-porphinato zinc(II) (denoted as ZnBPP-PECN), and 5-(4-carboxy-pyrimidinyl-ethlnyl)-10,20-biphenyl-porphinato zinc-(II) (denoted as ZnBPP-PMC1). The structures of chosen porphyrins and cluster were shown in Figures 1 and 2. As

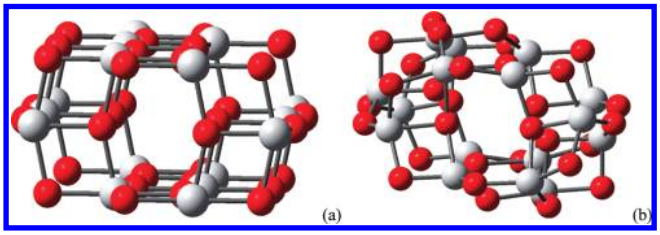

Figure 2. Anatase $Ti_{16}O_{32}$ cluster. (a) Unrelaxed crystal coordinates. (b) Fully optimized structure from DFT calculations.

reported by Wiberg and his co-workers,[22a] the coupling interaction difference could be ascribed to the electron density distributional difference on the attaching point. The distribution difference will bring changes in the interactions between the bridge and donor/acceptor. Specifically, it is true that large electron density concentration on the attaching points could make for large coupling for nondegenerate states. However, there also can be weak coupling and still delocalization (significant density across a bond) if the two species have nearly degenerate orbitals. For pyrimidine, the electron density distributes unequally on the rings, as there are more on the side of N atoms (so we designed the donor group attached to the C atom between the two N atoms). Compared with electron-rich phenyl, we predicted that the substitution of electron-deficient pyrimidine could lead to a stronger coupling interaction between the electron donor and the bridge groups and to a relative smaller coupling interaction between the anchoring and

dx.doi.org/10.1021/jp2109829 | J. Phys. Chem. C 2012, 116, 9166–9179

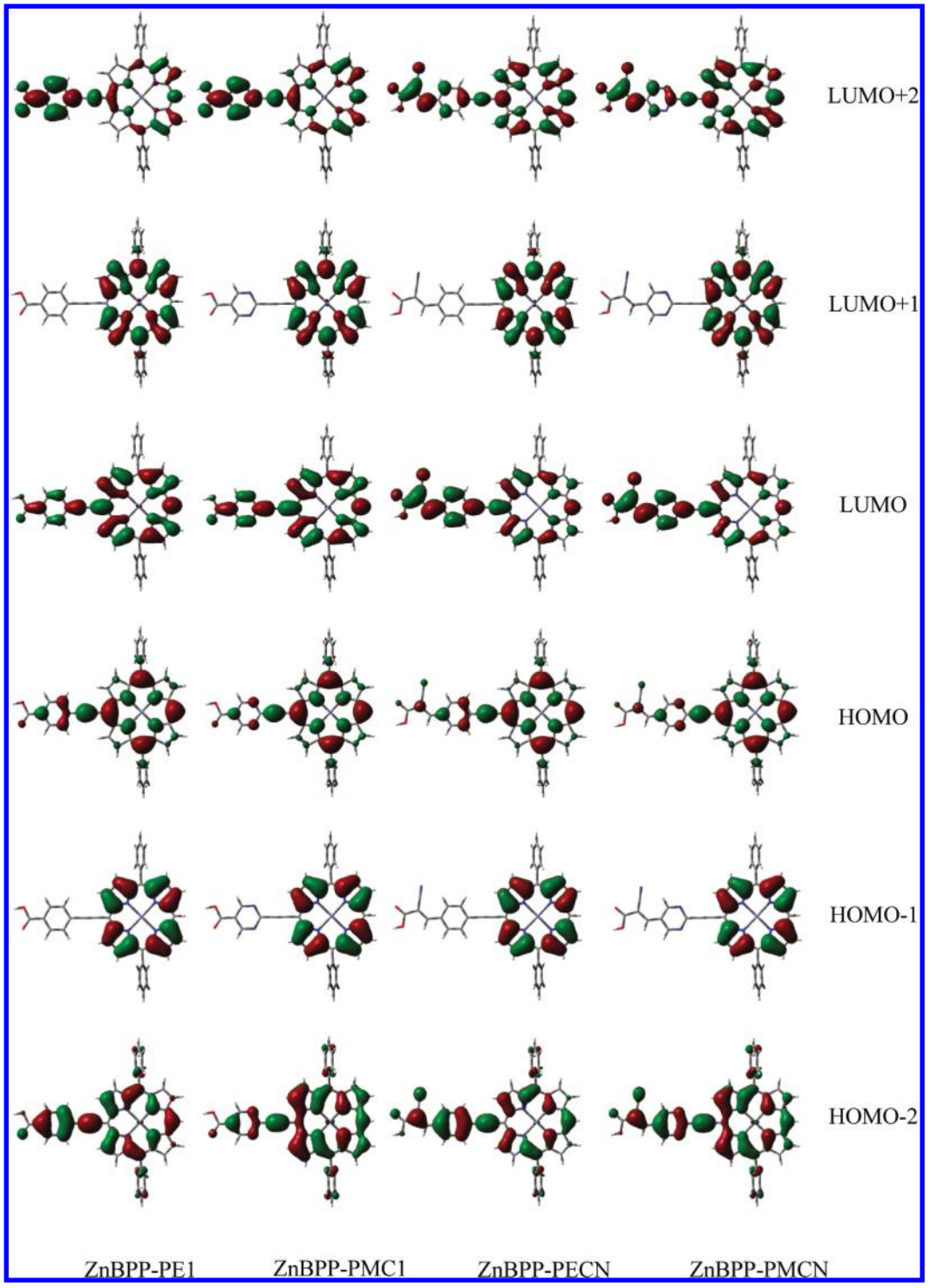

Figure 3. Molecular orbital spatial distribution.

bridge moieties. As pointed out by Persson,[19c,21a] stronger coupling could be beneficial to the electron transfer. From the qualitative point of view, therefore, there should be a lower energy barrier for electron transfer from the donor to the acceptor tunneling through the bridge group and a higher energy barrier for the reverse process. For ZnBPP-PECN and ZnBPP-PMCN, because of the presence of electron-withdrawing CN at the anchoring group, the frontier molecular orbitals were stabilized and extended out onto the substituent by conjugation. The extension of the conjugation of porphyrin to the substituent provides the possibility of electron transfer from porphyrin to the $Ti_{16}O_{32}$ cluster through the substituent. This suggests that a significant improvement on the performance of the solar cell should be achieved by using cyanoacrylic acid as an anchor group in the porphyrin sensitizer.[22b] On the whole, the fundamental donor−bridge−acceptor (D−B−A) system provides a stable and well-defined orientation of the sensitizers with respect to the nanoparticle surfaces, and the rigidity of the spacer ensures the control of distance between the light-harvesting centers and the TiO_2 surfaces.

dx.doi.org/10.1021/jp2109829 | J. Phys. Chem. C 2012, 116, 9166−9179

3.2. Frontier Molecular Orbital Spatial Distribution. Density functional calculations of molecules mentioned above showed a coplanar conformation between the zinc porphyrin moiety and the π-spacer connecting anchoring group. The coplanar push−pull system is favorable to the interaction between the electron donor group (EDG) and the conjugated π-spacer; furthermore, it is beneficial to the electron injection due to the modified appropriate energy level arising from the introduction of the π-conjugated spacer. From the frontier molecular orbital illustrated in Figure 3, we could see that the electron densities of highest occupied molecular orbitals (HOMOs) of these sensitizers are mainly populated on the ZnBPP (acted as EDG) and ethynyl moieties. The lowest unoccupied molecular orbitals (LUMOs) of ZnBPP-PMCN and ZnBPP-PECN are delocalized through the pyrimidyl and phenyl combined cyanoacrylic acid fragments. The LUMOs of ZnBPP-PE1 and ZnBPP-PMC1 are delocalized over the whole molecule. Comparison of LUMOs of ZnBPP-PE1 and ZnBPP-PECN indicated that the PECN unit is a bit more in electron density than the PE1 group. This difference should be ascribed to the different strengths of electron withdraw of the anchoring groups. The electron-deficient pyrimidinyl group combined with cyanoacrylic acid lowers the LUMO level much more than the phenylethynyl combined carboxylic acid does, which promotes the increase of electron densities localized on the acceptor group. To investigate the influence of acceptor fragments of sensitizers on the energy gap and electron density distribution, we calculated separately the energy levels of donor and acceptor fragments, and the data were listed in Table 1.

Table 1. Orbital Energy Levels of Porphyrin Molecules and Fragments

molecule	ε_{LUMO}	$\Delta\varepsilon_{HOMO-LUOMO}$	ε_{HOMO}
ZnBPP	−2.5385		−5.4109
PE1	−2.6302		−7.3813
PMC1	−3.0036		−7.9568
PECN	−3.4025		−7.1938
PMCN	−3.6958		−7.7674
ZnBPP-PE1	−2.8580	2.4764	−5.3344
ZnBPP-PMC1	−3.0365	2.4416	−5.4781
ZnBPP-PECN	−3.1461	2.2324	−5.3785
ZnBPP-PMCN	−3.3693	2.1496	−5.5189

Obviously, the LUMO energy levels of fragments are in the order of PE1 (−2.6302 eV) > PMC1 (−3.0036 eV) > PECN (−3.4025 eV) > PMCN (−3.6958 eV), all of them properly located below the LUMO energy level of the ZnBPP moiety (−2.5385 eV). Further, the same order of energy gaps was obtained when the conjunct sensitizers were considered: these are ZnBPP-PE1 (2.4764 eV) > ZnBPP-PMC1 (2.4416 eV) > ZnBPP-PECN (2.2324 eV) > ZnBPP-PMCN (2.1496 eV). It clearly suggested that the introduction of electron-deficient pyrimidine as the π-bridge has significant influences on decreasing the energy level of the LUMO and energy gap. Especially, a more obvious impact is yielded when the cyanoacrylic acid is introduced into the sensitizer. The position of the LUMO level and the nature of the acceptor group play an important role in determining the electronic coupling and therefore the efficiency of electron injection. In one instance, in the ruthenium bipyridine dyes,[3a] carboxylates have been proved to be favorable to electron injection by decreasing the LUMO energy of the bipyridine unit attached to the carboxylates, thereby ensuring the LUMO orbital of the dye is localized upon the bipyridine unit closest to the metal oxide surface. From the PDOS of the surface complexes in Figure 4, one can see that the HOMOs of complexes (upper valence band region) almost come from the porphyrin sensitizers, and the LUMOs (lower conductive band region) are mainly localized on the metal oxide with a small contribution from the adsorbates. In DSSCs, the small contribution plays a central role in heterogeneous electron transfer, and its electronic coupling with the surface is therefore particularly interesting.[21a] The more contributions from the LUMOs of adsorbates (LUMO(ads)) and the more electrons delocalized on the acceptors, the stronger the coupling interaction between the sensitizers and TiO_2 will be. The strength of the interfacial interaction could influence the electron injection from the photoexcited dyes to the TiO_2 surface. If there is a sufficiently strong interaction between the excited dye π^* levels and the TiO_2 substrate conduction band, the initial photoexcitation can be followed by an ultrafast electron transfer to the substrate conduction band and can retard competing processes, such as intramolecular thermalization.[21b] An adsorbate state with strong coupling to the surface can be expected to possess an orbital that is delocalized over the surface. From the calculated properties of selected unoccupied molecular orbitals (see Supporting Information, Table S9), we could get the quantitative contribution of adsorbate to the coupling interaction. Comparing the calculated data, it was found that there are more contributions (range from −4 to −2 eV) from ZnBPP-PMC1 than from ZnBPP-PE1, although they have the same anchoring group. These unoccupied molecular orbitals overlap the conduction band and strongly mix with the conduction band. So the coupling interaction between the sensitizer and TiO_2 cluster should be stronger for ZnBPP-PMC1 due to the adoption of pyrimidine. The conclusion coincided with the result that we got from analysis of the electron density distribution difference on attaching points. The estimation of coupling interaction using this approach is likely to be somewhat limited by the finite size of the nanocrystal model, which results in finite spacing of the band levels. As reported by Harima and co-workers,[23] the electron-withdrawing group CN of the dye has a strong interaction with the TiO_2 surface. For ZnBPP-PECN and ZnBPP-PMCN, the interaction cannot be fully considered on account of the limited size of the TiO_2 cluster model. In spite of this, the contributions of LUMOs of ZnBPP-PMCN and ZnBPP-PECN are larger than that of ZnBPP-PE1.

The charge transfer orientation is also associated with the electron density distribution of the HOMOs and the LUMOs of the sensitizers. In a simplified orbital description of electron transfer, the electron can be visualized as moving from the LUMO of ZnBPP to the LUMO of the semiconductor tunneling through the LUMO of the conjugated π-bridge. In porphyrin sensitizer systems, the energy drops of $LUMO_{donor}-LUMO_{acceptor}$ complied with the sequence of ZnBPP-PMCN (1.1573 eV) > ZnBPP-PECN (0.864 eV) > ZnBPP-PMC1 (0.4651 eV) > ZnBPP-PE1 (0.0918 eV), which indicated that the introductions of pyrimidine and cyanoacrylic acid are favorable for charge separation. The magnitude of energy barrier for reverse transfer should also follow this sequence; that is, the introduction of pyrimidine and cyanoacrylic acid could weaken the reverse transfer. The energy levels of the donor and acceptor moieties are thus very important for the effective charge separation and could affect the solar cell efficiency. To some extent, for these unattached sensitizers with

dx.doi.org/10.1021/jp2109829 | J. Phys. Chem. C 2012, 116, 9166−9179

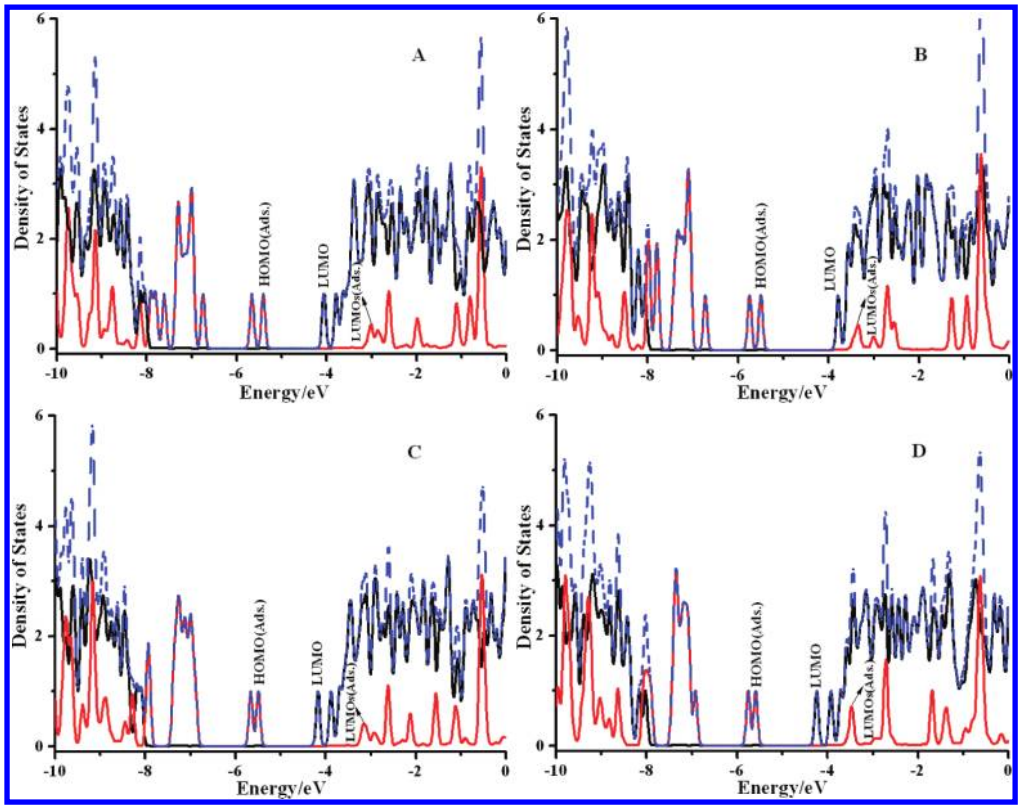

Figure 4. Total densities of states (TDOS) and projected DOS (PDOS) for bidentate adsorption on the $Ti_{16}O_{32}$ cluster of porphyrins sensitizers. A: ZnBPP-PE1. B: ZnBPP-PECN. C: ZnBPP-PMC1. D: ZnBPP-PMCN. TDOS (blue), PDOS for porphyrin (red). and TiO_2 (black).

the same donor (ZnBPP moiety) and different π-conjugated acceptors, the lower the LUMO energy level of the acceptor is, the more electron densities of the whole molecule will be localized at the acceptor part. This indicates more effective charge separation and higher photo-to-electric conversion efficiency. For example, inspection of Figure 3 suggested that the HOMO→LUMO excitation would shift the electron density distribution from the ZnBPP to the pyrimidinylethlnyl and phenylethylnyl connected cyanoacrylic acid moiety, sequentially facilitating efficient interfacial electron injection from excited dyes to the TiO_2 cluster.

From the discussions above, it is found that the cyanoacrylic acid ending is a better anchoring group for porphyrin sensitizers. For those acceptors with lower LUMO levels, the stronger the electron-withdrawing ability of the adjacent functional group, the lower the LUMO energy level of the sensitizers will be. That is to say, an electron-deficient pyrimidine system adjacent to the anchoring group, especially cyanoacrylic acid group, is more eximious to get lower LUMO level of the acceptor moiety and promote the electron movement from the porphyrin moiety to the acceptor, thereby improving the photo-to-electric conversion efficiency.

3.3. Performance of Spectral Absorption and Character of Photoinduced Charge Transfer. A measurement of the performance of DSSCs system is called incident photon to current conversion efficiency (IPCE). Simply, it is a function of light harvest efficiency (φ_{LHE}), electron injection efficiency (φ_{inject}), and charge collection efficiency (φ_{CC}) and can be expressed as[7b,13a,24]

$$\mathrm{IPCE} = \varphi_{LHE} \cdot \varphi_{inject} \cdot \varphi_{CC} \quad (1)$$

a. Absorption Behavior in THF Media. As a compromise between accuracy and basis set size, the absorption spectra calculations were performed by hybrid function B3LYP with 6-311G(d p) basis set. For most of the conjugated compounds, the excitation process often induces a charge separation (that actually needs extended basis sets). The calculated wavelengths (λ), oscillator strengths (f), and transition energies ($E_{\alpha\to\beta}$) for most of the relevant transitions of the electronic absorption bands in the tetrahydrofuran (THF) solvent were obtained from TD-DFT calculations.

For the calculation of the light-harvesting efficiency (LHE), eq 1[25] was used

$$\varphi_{LHE} = 1 - 10^{-f} \quad (2)$$

where f is the oscillator strength of the dye associated to the λ. The light-harvesting efficiency (LHE) of the dye has to be as high as possible to maximize the photocurrent response.

The simulated electronic spectra of sensitizers and the surface complexes were shown in Figure 5. The porphyrin sensitizers showed a series of bands between 300 and 700 nm due to $\pi\to\pi^*$ absorption of the conjugated macrocycle. The calculated absorption spectrum of the ZnBPP system paired PE1 unit agreed well with the previous experimental spectrum (the experimental absorption spectrum of ZnBPP-PE1 was inserted in Figure 5a). Comparing the absorption spectrum of ZnBPP-PE1 with those of ZnBPP-PMCN, ZnBPP-PECN, and ZnBPP-PMC1 revealed that the Q band of those novel designed sensitizers yielded a bathochromic shift. The locations of absorption peaks are 591, 596, 643, and 663 nm for ZnBPP-PE1 (f = 0.382), ZnBPP-PMC1 (f = 0.455), ZnBPP-PECN (f = 0.992), and ZnBPP-PMCN (f = 1.047) in the Q band region, respectively. The calculated light-harvesting efficiencies (LHE)

dx.doi.org/10.1021/jp2109829 | J. Phys. Chem. C 2012, 116, 9166–9179

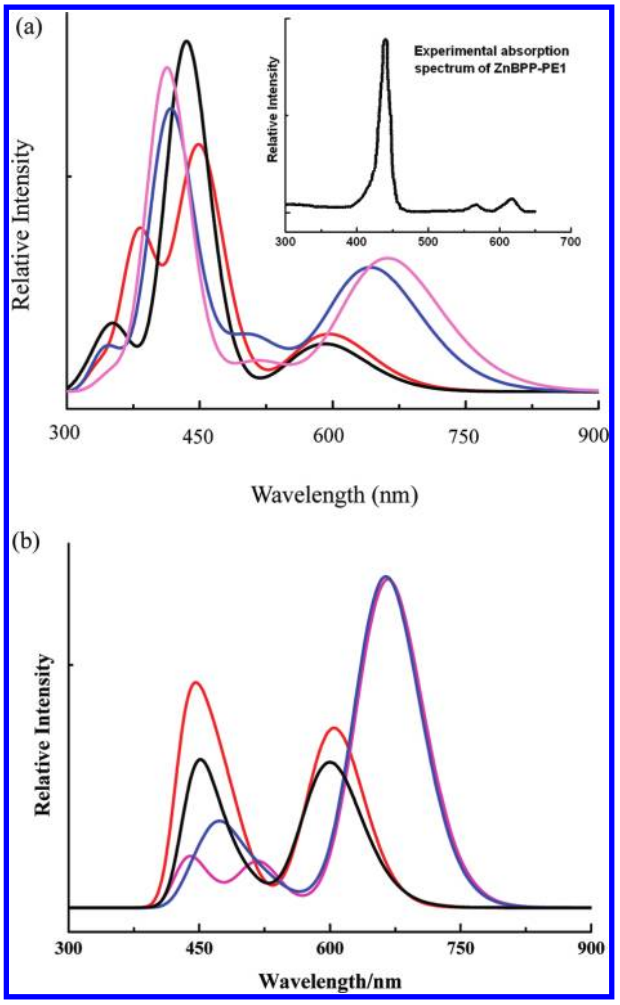

Figure 5. (a) Simulated spectral absorption of porphyrin sensitizers. Inset: the experimental absorption spectrum of the ZnBPP-PE1 porphyrin sensitizer.[13a] (b) The corresponding simulated spectral absorption of the surface complexes on $Ti_{16}O_{32}$ cluster: ZnBPP-PE1 (black), ZnBPP-PMC1 (red), ZnBPP-PECN (blue), ZnBPP-PMCN (pink).

are 0.5850, 0.6492, 0.8982, and 0.9102. Obviously, ZnBPP-PMCN obtained a stronger and more red-shifted absorption of the Q band relative to the ZnBPP-PE1 sensitizer. The surface complexes of ZnBPP-PECN (f = 1.252) and ZnBPP-PMCN (f = 1.223) have more outstanding spectral absorption in the Q band region relative to the unattached ones. Sensitizer ZnBPP-PMC1 showed obvious split and broadening in the *Soret* band, indicating there is a strong interaction between the ZnBPP and pyrimidinylethlnyl moiety. The introductions of the electron-deficient pyrimidine and cyanoacrylic acid sharply decreased the HOMO−LUMO energy gap (see Table 1), which is also responsible for the significant red shift of the absorption spectrum. Through the comparison of spectral absorption between ZnBPP-PE1 and ZnBPP-PECN, the extended absorption spectrum of ZnBPP-PECN indicates that the cyanoacrylic acid is more outstanding in lowering the LUMO energy level and narrowing the energy gap than carboxylic acid because of its stronger electron withdraw and better π-conjugated effect with the adjacent phenyl system. By the same token, the cyanoacrylic acid combined pyrimidine is more excellent in extending the optical absorption than combined phenyl. As we mentioned above, one drawback of porphyrin as sensitizer used in DSSCs is the absorption vacancy between the *Soret* and Q bands that decreases the light-harvesting efficiency. For ZnBPP-PECN and ZnBPP-PMCN, a new absorption band between Q and *Soret* bands appeared. This absorption peak is considered as a result of the insert of the cyanoacrylic acid. The extension of the conjugation of porphyrin to the substituent provides the possibility of electron transfer from ZnBPP to the substituent, which could induce extra absorption bands. In addition, adoption of the electron-donating group onto the periphery of the zinc-porphyrin system is also revealed to be able to lead to novel dyes with further red-shifted near-infrared (NIR) absorption bands, relevant attempts usually imposed simultaneously.[13c,d]

b. Photoinduced Charge Transfer Characters. To illustrate visually the electron transition, the electron density difference plots of electron transitions were mapped. The total electron density difference between the initial and final states ($\sum\partial_{\alpha\to\beta}$) is expressed as a sum of molecular orbital transitions involving each participating excitation, $\alpha\to\beta$.

$$\partial_{\alpha\to\beta} = \frac{C^2_{\alpha\to\beta}}{\sum C^2_{\alpha\to\beta}}(\rho_\alpha - \rho_\beta) \tag{3}$$

$C_{\alpha\to\beta}$ is the orthogonal coefficient in the TD-DFT equation, and then $C^2_{\alpha\to\beta}/\Sigma C^{\,2}{}_{\alpha\to\beta}$ represents the contribution of the electron transition model to this absorption peak. ρ_α and ρ_β are the electron densities of the participating molecular orbital relative to the transitions.

$$\rho_{(r)} = \sum_i \eta_i |\varphi_i(r)|^2 = \sum_i \eta_i |C_{j,i}\chi_j(r)|^2 \tag{4}$$

where η_i is the occupation number of orbital i, and χ is basis function. C is the coefficient matrix, and the element of the ith row, jth column corresponds to the expansion coefficient of orbital j with respect to basis function i. The electron density difference between the initial and final states is the linear combination of various electron transition models. For the donor−bridge−acceptor porphyrin system, in a simplified orbital description of electron transition (ET), the electron could be visualized as moving from the ZnBPP group to the anchor group tunneling through the bridge moiety. The bridge moiety guides the light absorption region of the DSSCs and subsequently the scale of the electron injection from the excited state of the dyes to the semiconductor surface.

The absorption spectra in the first visible region of porphyrin sensitizers, abbreviated as Vis-1 (550−700 nm), were assigned to the Q regions of these porphyrin sensitizers. The main electron transition comes from HOMO→LUMO, coupling with HOMO-1 → LUMO+1. As was shown in Table 2, only the electron transition models with the contribution larger than 5.0% and the oscillation strength larger than 0.1 were taken into account, and the electron densities move from the blue area to the green area. From the molecular orbital spatial distribution (displayed in Figure 3), the electron distribution of LUMO+1 was localized entirely on the ZnBPP group. It is evident that the electron density transfer from the ZnBPP group to the acceptor moiety stems from the transition of HOMO → LUMO rather than that of HOMO-1 → LUMO+1 in this region. The efficiency of electron density movement is related to both optical absorption intensity and available electron transition and could be estimated from the light-harvesting efficiency and the coefficient of effectual electron transition. The applicability and reliability should be based on the simplexes of electron

dx.doi.org/10.1021/jp2109829 | J. Phys. Chem. C 2012, 116, 9166−9179

Table 2. Electron Density Difference Plots of Electronic Transitions[a] (Assignment: H = HOMO, L = LUMO, L+1 = LUMO+1, H-1 = HOMO-1, etc.)

ZnBPP-PMCN	ZnBPP-PE1
$\Phi_1 \approx 0.691\Psi_{H\rightarrow L}$ 663nm $f = 1.0467$ Main Transitions: H→L (95%)	$\Phi_1 \approx -0.306\Psi_{H-1\rightarrow L+1} + 0.635\Psi_{H\rightarrow L}$ 591nm $f=0.382$ Main Transitions: H-1→L+1 (19%) H→L (81%)
$\Phi_2 \approx 0.394\Psi_{H-1\rightarrow L+2} + 0.570\Psi_{H\rightarrow L+1}$ 517nm $f=0.184$ Main Transitions: H-1→L+2 (31%) H→L+1 (65%)	$\Phi_2 \approx 0.544\Psi_{H-1\rightarrow L+1} + 0.278\Psi_{H\rightarrow L} + 0.325\Psi_{H\rightarrow L+2}$ 437nm $f=1.6593$ Main Transitions: H-1→L+1 (59%) H→L (15%) H→L+2 (21%)
$\Phi_3 \approx 0.435\Psi_{H-2\rightarrow L} + 0.424\Psi_{H-1\rightarrow L+2} - 0.288\Psi_{H\rightarrow L+1}$ 423nm $f=1.185$ Main Transitions: H-2→L (38%) H-1→L+2 (36%) H→L+1 (17%)	$\Phi_3 \approx 0.513\Psi_{H-1\rightarrow L} - 0.460\Psi_{H\rightarrow L+1}$ 433nm $f=1.1525$ Main Transitions: H-1→L (53%) H→L+1 (42%)
$\Phi_4 \approx -0.125\Psi_{H-1\rightarrow L+1} + 0.427\Psi_{H\rightarrow L+2}$ 407nm $f=1.3976$ Main Transitions: H-1→L+1 (56%) H→L+2 (37%)	$\Phi_4 \approx 0.529\Psi_{H-5\rightarrow L} + 0.385\Psi_{H-1\rightarrow L+2}$ 361nm $f=0.2107$ Main Transitions: H-5→L (56%) H-1→L+2 (30%)
$\Phi_5 \approx -0.187\Psi_{H-10\rightarrow L} + 0.279\Psi_{H-6\rightarrow L} - 0.312\Psi_{H-4\rightarrow L} + 0.399\Psi_{H-2\rightarrow L} - 0.243\Psi_{H-1\rightarrow L+2} + 0.196\Psi_{H\rightarrow L+1}$ 389nm $f=0.124$ Main Transitions: H-10→L (7%), H-6→L (16%), H-4→L (19%), H-2→L (32%), H-1→L+2 (12%),H→L+1 (8%)	$\Phi_5 \approx 0.281\Psi_{H-4\rightarrow L} + 0.582\Psi_{H-2\rightarrow L+1}$ 342nm $f=0.23$ Main Transitions: H-4→L (16%) H-2→L+1 (68%)
ZnBPP-PMC1	ZnBPP-PECN
$\Phi_1 \approx -0.288\Psi_{H-1\rightarrow L+1} + 0.643\Psi_{H\rightarrow L}$ 596nm $f=0.455$ Main Transitions: H-1→L+1 (17%) H→L (83%)	$\Phi_1 \approx 0.681\Psi_{H\rightarrow L} + 0.176\Psi_{H-1\rightarrow L+1}$ 643nm $f=0.9921$ Main Transitions: H→L (93%) H-1→L+1 (6%)

ZnBPP-PMC1	ZnBPP-PECN
$\Phi_2 \approx 0.492\Psi_{H-1\rightarrow L+1} + 0.250\Psi_{H\rightarrow L} + 0.438\Psi_{H\rightarrow L+2}$ 450nm $f=1.2714$ Main Transitions: H-1→L+1(48%) H→L (12%), H→L+2 (38%)	$\Phi_2 \approx -0.376\Psi_{H-1\rightarrow L+1} + 0.577\Psi_{H\rightarrow L+2}$ 514nm $f=0.2756$ Main Transitions: H-1→L+1 (28%) H→L+2 (67%)
$\Phi_3 \approx -0.409\Psi_{H-1\rightarrow L} - 0.295\Psi_{H-1\rightarrow L+2} + 0.492\Psi_{H\rightarrow L+1}$ 448nm $f=0.6935$ Main Transitions: H-1→L (34%) H-1→L+2 (18%) H→L+1 (48%)	$\Phi_3 \approx 0.385\Psi_{H-1\rightarrow L} + 0.397\Psi_{H-1\rightarrow L+2} + 0.439\Psi_{H\rightarrow L+1}$ 499nm $f=0.1712$ Main Transitions: H-1→L (30%) H-1→L+2 (31%) H→L+1 (38%)
$\Phi_4 \approx -0.370\Psi_{H-2\rightarrow L} - 0.328\Psi_{H-1\rightarrow L+1} + 0.470\Psi_{H\rightarrow L+2}$ 391nm $f=0.3585$ Main Transitions: H-2→L (27%) H-1→L+1 (22%) H→L+2 (44%)	$\Phi_4 \approx 0.456\Psi_{H-2\rightarrow L} - 0.434\Psi_{H-1\rightarrow L+1} - 0.296\Psi_{H\rightarrow L+2}$ 427nm $f=1.2541$ Main Transitions: H-2→L (42%) H-1→L+1 (38%) H→L+2 (18%)
ZnBPP-PMC1	ZnBPP-PECN
$\Phi_5 \approx 0.622\Psi_{H-1\rightarrow L+2} + 0.242\Psi_{H\rightarrow L+1}$ 380nm $f=0.8525$ Main Transitions: H-1→L+2 (77%) H→L+1 (12%)	$\Phi_5 \approx 0.563\Psi_{H-1\rightarrow L+2} - 0.374\Psi_{H\rightarrow L+1} - 0.152\Psi_{H-1\rightarrow L}$ 408nm $f=1.2372$ Main Transitions: H-1→L+2 (63%) H→L+1 (28%) H-1→L (5%)
	$\Phi_6 \approx 0.627\Psi_{H-2\rightarrow L+1} - 0.163\Psi_{H-6\rightarrow L+1}$ 347nm $f=0.1981$ Main Transitions: H-2→L+1 (79%) H-6→L+1 (5%)

[a](Isovalue: 4×10^{-4} e·au^{-3}.) Only the electronic transition models with the contribution larger than 5.0% and the oscillation strength larger than 0.1 were taken into account. Electron densities move from the blue area to the green area.

transition. Such as the *Q* bands, the calculated light-harvesting efficiencies of ZnBPP-PMCN, ZnBPP-PECN, ZnBPP-PMC1, and ZnBPP-PE1 were 0.9102, 0.8982, 0.6492, and 0.5850, and the effectual electron transition contributions were 0.95, 0.93, 0.83, and 0.81, respectively. Obviously, for sensitizer ZnBPP-PE1, there is a poor spectral absorption and relatively limited charge separation in this long-wavelength region. It must be one of the results that directly restricts its performance and applicable efficiency in DSSCs. For ZnBPP-PMC1, it brings some improvement due to the pyrimidinyl-substituted phenyl. ZnBPP-PMCN showed strong spectral absorption and distinct charge separation in this region. The pyrimidine π-spacer combined cyanoacrylic acid anchoring group plays an important part in the increase of charge separation efficiency in this region due to the lower energy gap and stronger ability of electron withdrawing. This character is important for photosensitizers to make full use of light with longer wavelength, even the near-infrared spectral absorption, to achieve effective electron movements. More promising photosensitizes should be designed based on these properties.

In the region of Vis-2 (480−550 nm), the calculated results showed that both ZnBPP-PECN and ZnBPP-PMCN have new absorption peaks with relatively weak intensity, which are, respectively, located at 514 and 517 nm. The electron transitions associated to the new absorption peaks could result in electron transfer from the porphyrin system to the π-spacer bridged to the cyanoacrylic acid, as shown in the plots (see Table 2). It hints that the anchoring group adjacent to the π-spacer moiety, especially the cyanoacrylic acid group, is helpful to improve the performance in optical absorption of sensitizers. The absorption vacancy between *Soret* and *Q* bands for ZnBPP-PE1 andZnBPP-PMC1 naturally limits the charge transfer and influences the conversion efficiency.

The absorption spectra in region Vis-3 (400−480 nm) were assigned to the *Soret* bands of photosensitizers. Usually, promising sensitizers should have the strongest absorption in this region (hence the highest light-harvesting efficiency), which is crucial to the electron transition. In our calculated results, there are two absorption components in this region for these designed sensitizers individually, and these two components are located so close that only one wide *Soret*

dx.doi.org/10.1021/jp2109829 | J. Phys. Chem. C 2012, 116, 9166−9179

absorption band could be observed. The available electron transitions which drive electron movements from donor to acceptor groups must be related to the final states of LUMO and LUMO+2. From the plots of electron density difference of ZnBPP-PE1 in this region, there is a lack of effective electron movement corresponding to the absorption located at 433 nm, and the scene gets better at 437 nm. From the discussion of frontier molecular orbital spatial distribution, we know that the acceptor moiety locates its LUMO energy level at a lower position, which consequentially makes for a much more resultful electron movement from the donor group to acceptor. Analogously, the electron movements corresponding to the strong absorptions are more effective for ZnBPP-PMCN, ZnBPP-PMC1, and ZnBPP-PECN relative to ZnBPP-PE1 in this region. From the plots in Table 2, the sensitizer ZnBPP-PE1 displays the lowest charge separation efficiency, although it obtained the strongest spectral absorption (f = 1.6593) in this region. The awkward situation of poor electron transport in this region directly decreased the phototo-electric efficiency of ZnBPP-PE1. This case should be greatly changed when the cyanoacrylic acid substituted the carboxylic acid as the anchoring group or the electron-deficient pyrimidine substituted the phenyl. The charge separations are more evident in this region for ZnBPP-PECN and ZnBPP-PMC1 than ZnBPP-PE1. There are relatively higher electron separation efficiencies for ZnBPP-PECN (f = 1.2372, 1.2541) and ZnBPP-PMC1 (f = 1.2714, 0.6935), although the absorption intensities were lower than ZnBPP-PE1 in this region. As for ZnBPP-PMC1 and ZnBPP-PMCN (f = 1.185, 1.3976), the comparability of the electron separation behaviors and the discrepancies of electronic absorption behaviors indicate that the effect of different anchoring groups on the performance is mainly embodied in the light-harvesting efficiency rather than the electron separation efficiency. We here can conclude tentatively that the cyanoacrylic acid and pyrimidine groups play a central role in enhancing the performance in DSSCs.

The absorption spectra in the UV−vis region (300−400 nm) were assigned to the N bands (also can be assigned to a split of *Soret* band) of sensitizers with a higher-frequency region adjacent to the *Soret* bands. Generally, their absorption intensities are relatively smaller than the *Soret* bands' ones. For ZnBPP-PMC1, a strong N peak appears in the absorption spectrum, which is ascribed mainly to the electron transition of HOMO-1 → LUMO+2, bringing an electron movement from the ZnBPP group to the pyrimidine connected cyanoacrylic acid ending. As shown in Table 2, the N band of ZnBPP-PMCN also leads to electron transfer from the donor to acceptor, while the nature of this absorption is complicated because it consists of several electron transitions with HOMO-10 → LUMO (7%), HOMO-6 → LUMO (16%), HOMO-4 → LUMO (19%), HOMO-2 → LUMO (32%), HOMO-1 → LUMO +2 (12%), and HOMO → LUMO+1 (8%). It is true that these transitions could make for available electron movement except the HOMO → LUMO+1 (8%). In addition, the electron movement related to the N band of ZnBPP-PECN is from the PECN moiety to the ZnBPP group (the absorption at 347 nm); it also can be seen from the absorption at 347 nm of ZnBPP-PE1 as displayed in the plot. The phenomena are derived from the electron transitions to the LUMO+1. As the final state of electron transition, the electron distribution of LUMO+1 is entirely located at the porphyrin cycle. From the comparison of electron density difference plots of the sensitizers with and without the pyrimidine, we could conclude that the existence of an electron-deficient pyrimidine played a key role in the unidirectional electron movements. These results could be ascribed to the stronger coupling interaction between the donor group and the bridge, while the relatively smaller coupling is between the anchoring group and bridge group. In other words, there is a low energy barrier for electron transport from the donor to the acceptor tunneling through the bridge group and a relatively higher energy barrier for the reverse electron movements. The coupling interaction difference could arouse resultful charge separation and unfavorable reversal of charge movements.[11,21] The result provides a clear way for designing molecules of effective charge separation and limited electron recombination.

From the detailed analysis above, we can clearly know about the intrinsic characters of the photoinduced charge transfer from donor to acceptor groups. For these porphyrin sensitizers, all kinds of absorptions stem from varied $\pi \rightarrow \pi^*$ electron transitions. From the electron density difference plots, we can infer that not all electron transitions could make for the effective electron transports from the donor to the acceptor group. For instance, the ZnBPP-PE1 sensitizer has a strong absorption at 437 nm yet a limited quantity of electron movement from ZnBPP to the PE1 group. There is an evident electron separation that appears at 361 nm; nevertheless, it achieves limited light absorption. What is worse, a reversal of electron movement from the PE1 moiety to the ZnBPP group is observed for the absorption located at 342 nm, which must decrease the performance of sensitizers. On the other hand, although the ZnBPP-PMC1 obtained relatively worse spectral absorption than the other porphyrin derivatives presented here, more prominent unidirectional electron movement was obtained, as shown in Table 2. The ZnBPP-PMCN and ZnBPP-PECN were designed for a special purpose to reveal the important role pyrimidine and cyanoacrylic acid played in the performance of electron movement. On the basis of the comprehensive analysis and comparison above, the ZnBPP-PMCN and ZnBPP-PMC1 obtained more excellent unidirectional electron movement from the donor to acceptor than ZnBPP-PECN and ZnBPP-PE1 without considering the adsorption on the TiO_2 surface. So, the performance of sensitizers not only relies on the extrinsic spectral absorption intensities but also depends on the intrinsic character of electron transitions. To further design and develop more promising sensitizers for DSSCs, appropriate D−B−A systems that can obtain high light-harvesting efficienc and large spectrum overlap combined effective electron movements from the electron donor to acceptor are required. To confirm the reliability and give an insight into the charge separation in DSSC systems, the electron density differences of surface complexes with bidentate mode were calculated for parallel comparisons (the electron density difference plots of surface complexes were presented in the Supporting Information). The results supported the conclusion that electron-deficient pyrimidine plays a central role in unidirectional electron transports and improves the charge separation efficiency. The calculated results also showed that for the surface complexes there are more electron transitions with high intensities in porphyrin sensitizers bridged to the pyrimidine spacer.

3.4. Performance of Sensitizers in Regeneration and Electron Injection. Structural and electronic properties of photosensitizers have an important effect on the performance of DSSCs, and any works about sensitizer synthesis and design should be premised on obtaining comprehensive information

dx.doi.org/10.1021/jp2109829 | J. Phys. Chem. C 2012, 116, 9166−9179

about them. We calculated several electronic properties of photosensitizers which were used to elucidate the greater suitability of the electron-deficient pyrimidine system for the π-spacer. The electron injection efficiencies were evaluated by calculating the Gibbs energy changes of electron injection of sensitizers. The theoretical results of driving force support the conclusions mentioned above and ensures the rationality of the calculated electron injection efficiencies. Furthermore, the regeneration efficiencies of oxidized dyes were also calculated, and this provided the evidence for screening of promising sensitizers for DSSCs.

a. Calculation of Redox Potential. To obtain optimal electron injection and regeneration of the oxidized dyes, the redox potentials of dyes should match the semiconductor and electrode, which is fundamentally important to the function of DSSCs. The redox potential of the system in the ground state, $E_{\text{redox(dye)}}$, versus the normal hydrogen electrode (NHE) for the one-electron redox couple, is given by the Nernst equation and can be written in the energy scale as eq 5.[24]

$$E_{\text{redox(dye)}} = \frac{\Delta G_{(\text{aq})} - \Delta G_{(\text{NHE})}}{nF} \quad (5)$$

The value of $\Delta G_{(\text{aq})}$ is Gibbs free energy change due to the oxidation of the dye in solution. We can calculate it according to the Born−Haber cycle, as shown in Scheme 1. $\Delta G_{(\text{NHE})}$, the

Scheme 1. Thermodynamic Cycle Used to Calculate the Redox Potentials

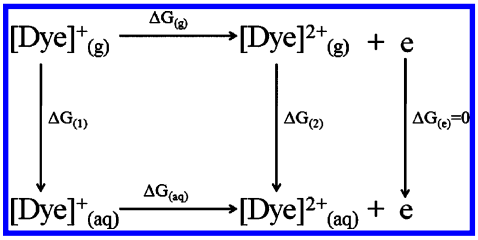

Gibbs free energy change of the normal hydrogen electrode, takes the standard value of −4.44 eV.[26] F denotes the Faraday constant with 23.06 kcal·mol^{-1}·V^{-1}. n is the number of electrons involved in the redox couple $[\text{dye}]^{2+}/[\text{dye}]^{+}$ (here n = 1).

b. Evaluation of Electron Injection. The value of φ_{inject} depends on the coupling between the photosensitizer and semiconductor. Actually, the thermodynamic driving force (D) could reflect φ_{inject} related to the corresponding vertical excitation.

$$\varphi_{\text{inject}} \propto D \quad (6)$$

The driving force (D) can be calculated by eq 7[24]

$$D = |E_{\text{redox(dye)}} - \Delta E - E_{\text{CB}}| \quad (7)$$

where ΔE is the vertical excitation energy which could be obtained from TD-DFT calculation. The value of E_{CB} is the conduction band edge of TiO_2 (−0.44 V vs NHE). We can also calculate the Gibbs free energy change of electron injection (ΔG_{inject}) to reflect the overall electron injection efficiency[25,27]

$$\Delta G_{\text{inject}} = E_{\text{OX(dye*)}} - E_{\text{CB}} \quad (8)$$

To calculate ΔG_{inject}, there are two strategies to obtain the oxidized potential of the first excited state (S_1), $E_{\text{OX(dye*)}}$. In the first strategy, we get $E_{\text{OX(dye*)}}$ only if we consider the excitation is followed by electron injection immediately. $E_{\text{OX(dye*)}}$ could be calculated by eq 9[25]

$$E_{\text{OX(dye*)}} = E_{\text{OX(dye)}} - E_{\lambda_{\text{max}}} \quad (9)$$

$E_{\text{OX(dye)}}$ is the oxidized potential of the ground state, and we evaluated it from the HOMO energy level of the sensitizer.[13c] Actually, for dye regeneration, the oxidized state level of the photosensitizer in the ground state must be more positive than the redox potential of electrolyte. $E_{\lambda\text{max}}$ is the vertical transition energy from the ground state to excited states. The vertical transition energy is frequently associated with the wavelength maximum in the absorption spectra. It is much more accurate than adopting the HOMO−LUMO energy gap. As we know, the excited state is usually formed by more than one-electron excitation and not just derived from the transition between HOMO and LUMO, though generally, it is the major contribution. The vertical transition process denoted 1 is shown in Scheme 2.

Scheme 2. Schematic Potential Energy Surfaces for Ground and First Excited States of Sensitizer, Illustrating the Energies and Displacements Used in Equations 9−12

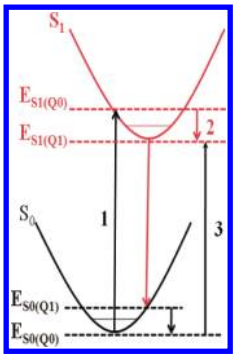

In the second strategy, the transition process that we focus on customarily is an adiabatic process for photosensitizers, and it means that there is enough time to achieve the stable state for the excited dye molecule. The relaxation of excited state denoted 2 is also shown in Scheme 2. The electron injection is performed following the relaxation of the excited dye, and the experimenters commonly assume that electron injection dominantly occurs after relaxation.[27,28] To obtain the value of $E_{\text{OX(dye)*}}$, a calculation of the geometrical relaxation energy for the S_1 state as it proceeds from ground-state geometry to that of the S_1 geometry is a prerequisite. Neglecting zero-point affects the energy difference between the equilibrium geometries of the ground and the first excites states. The 0−0 transition energy (denoted as 3 in Scheme 2) is obtained[25,27]

$$E_{\text{OX(dye*)}} = E_{\text{OX(dye)}} - E_{\text{0-0(dye)}} \quad (10)$$

$E_{\text{0-0(dye)}}$ in eq 10 can be expressed as[25,27]

$$E_{\text{0-0(dye)}} = E_{\lambda_{\text{max}}} - \Delta E_{\text{reorg}(S_1)} \quad (11)$$

The S_1 reorganization energy ($\Delta E_{\text{reor(S1)}}$) is the difference between $E_{S1(Q1)}$ and $E_{S1(Q0)}$ (both of them are S_1 energies calculated at S_0 and S_1 equilibrium geometries, respectively). That is[25]

$$\Delta E_{\text{reorg}(S_1)} = E_{S_1(Q_0)} - E_{S_1(Q_1)} \quad (12)$$

In addition, the charge recombination from the reduced TiO_2 nanoparticle to the oxidized porphyrin and the efficiency of dye

dx.doi.org/10.1021/jp2109829 | J. Phys. Chem. C 2012, 116, 9166−9179

Table 3. Estimated and Experimental $\Delta G_{(aq)}$, E_{redox}, $E_{\lambda max}$, E_{reorg}, E_{0-0}, and f for Porphyrin Sensitizers

scheme	$\Delta G_{(aq)}$[a]	E_{redox}[b] (Exp)	$E_{\lambda max}$[c] (Exp)	E_{reorg}[d]	E_{0-0}[e]	f[f]
ZnBPP-PE1	6.2204	1.7804 (1.81[g])	2.8371 (2.8242[g])	0.1115	2.7256	0.3820/1.6593
ZnBPP-PMC1	6.3183	1.8784	2.7552	0.1204	2.6348	0.4550/1.2714
ZnBPP-PECN	6.2340	1.7940	2.9036	0.1536	2.7500	0.9921/1.2541
ZnBPP-PMCN	6.3347	1.8947	3.0449	0.1542	2.8907	1.0467/1.3976

[a]Calculated Gibbs free energy change ($\Delta G_{(aq)}$, in au) due to the oxidation of the dyes in aqueous solutions. [b]Redox potential (E_{redox} vs NHE, in V). [c]The energy (in eV) corresponds to the maximum wavelength of spectral absorption. [d]The reorganization energy (in eV) of the first excited state. [e]The 0−0 transition energy (in eV). [f]The oscillation strength related to the Q band and B band, respectively. [g]Reference 13a.

Table 4. Estimated and Experimental $E_{OX(dye)}$, $E_{OX(dye^*)}$, $\Delta G_{unrelax}$, ΔG_{relax}, D, and LHE for Porphyrin Sensitizers

scheme	$E_{OX(dye)}$[a] (Exp)	$E_{OX(dye^*)}$[b] (Exp)	$\Delta G_{unrelax}$[c] (Exp)	ΔG_{relax}[d]	D[e]	LHE[f]
ZnBPP-PE1	0.8944 (1.07[g])	−1.9426/−2.0541 (−1.7542[g]/N.a.)	−1.5027 (−1.314[g])	−1.6142	0.1225/0.6128	0.5850/0.9780
ZnBPP-PMC1	1.0381	−1.7170/−1.8374	−1.2770	−1.3974	0.2382/0.4368	0.6492/0.9465
ZnBPP-PECN	0.9385	−1.9650/−2.1186	−1.5250	−1.6787	0.3059/0.6695	0.8982/0.9443
ZnBPP-PMCN	1.0789	−1.9659/−2.1200	−1.5259	−1.6801	0.4633/0.7101	0.9102/0.9600

[a]Calculated the oxidized potential (vs NHE, in V) of ground state ($E_{OX(dye)}$). [b]The oxidized potential of the first excited state ($E_{OX(dye^*)}$) following unrelax/relax path for dyes. [c]The Gibbs free energy (vs. NHE, in V) of election injection following unrelax path ($\Delta G_{unrelax}$). [d]The Gibbs free energy (vs. NHE, in V) of election injection following relax path (ΔG_{relax}). [e]The driving force (D, in V) of electron injection related to the electronic transition in the Q/B band. [f]The light-harvesting efficiency (LHE) corresponding to the Q/B band. [g]Reference 13a. n.a. denotes no available value.

regeneration by the oxidation of electrolyte were considered, which have direct impacts on the value of charge collecting efficiency.[29a] Experimentally, the intensity modulated photovoltage spectroscopy (IMVS) and intensity modulated photocurrent spectroscopy (IMPS) are used to evaluate the charge collection efficiency (φ_{CC}) of DSSCs.[29b]

To address optimal energy levels in a paired donor/acceptor of the light-harvesting system, the optical excitation energy gaps of both the donor and the acceptor should be engineered to match the photon energy, as both can harvest photon and incur charge separation at the donor/acceptor interface. First, the oxidized state level of the photosensitizer must be more positive than the oxidized potential of the electrolyte to facilitate the regeneration of the oxidized dyes. Second, the excited-state level of the photosensitizer should be higher in energy than the conduction band edge of the semiconductor conduction band (CB), so that an efficient electron transfer process from the excited dye to the CB of the semiconductor can take place. This efficiency of the charge separation is central to the performance of dye-sensitized solar cells.

On the basis of the discussion of the above theoretical details, these parameters were calculated, and the results were presented in Tables 3 and 4. Our purpose is to illustrate how the pyrimidine and cyanoacrylic acid affect the regeneration of the oxidized dyes and the electron transfer process through modifying these energy and potential levels. These processes are important to determine the photo-to-electric efficiency of DSSCs. The calculated data showed that the oxidation potentials of ground states for these porphyrin sensitizers are larger than that of the I^-/I^-_3 redox couple, as shown in Figure 6. Compared to the oxidation potential of these sensitizers, the results fulfill the sequence of ZnBPP-PMCN > ZnBPP-PMC1 > ZnBPP-PECN > ZnBPP-PE1 > I^-/I^-_3. The calculated regeneration driving forces of ZnBPP-PE1, ZnBPP-PECN, ZnBPP-PMC1, and ZnBPP-PMCN are 0.5944, 0.6385, 0.7381, and 0.7789 V, respectively. This may be compared to 0.70 V for the conventional N719 complex (bis(tetrabutylammonium)-*cis*-(dithiocyanato)-*N*,*N*′-bis(4-carboxylato-4′-carboxylic acid-2,2′-bipyridine) ruthenium(II)).[3b] The anodic displacements showed that electron-deficient pyrimidine could promote the

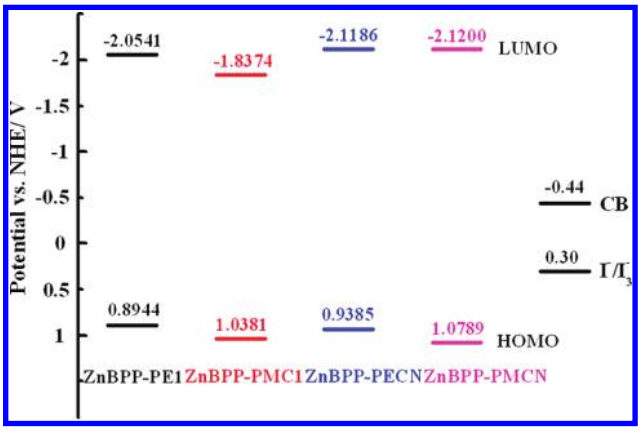

Figure 6. Schematic energy levels of porphyrins ZnBPP-PE1, ZnBPP-PMC1, ZnBPP-PECN, and ZnBPP-PMCN. HOMO = $E_{OX(dye)}$, LUMO = $E_{OX(dye^*)}$. $E_{OX(dye^*)}$ was calculated with eq 10.

regeneration of oxidized dyes. The effective regeneration of oxidized dyes is beneficial to the unidirectional charge transport and avoiding the charge recombination. Alebbi and co-workers[30] reported that inefficient regeneration could limit the device photocurrent. Their study focused upon a comparison of osmium- and ruthenium-based sensitizers. The osmium dye obtained a smaller ground state oxidation potential, resulting in the decrease of driving force for the regeneration, although it exhibited stronger near-infrared absorption. The lower photocurrent of the osmium-based devices was assigned to slower iodide regeneration of the dye ground state. From the present results, we can get that the sensitizers combining the electron-deficient pyrimidine have a vantage of generation of oxidized dyes. Furthermore, the π-bridge that adopted the cyanoacrylic acid is better than carboxylic acid ending. It can facilitate the dyes adsorbed on the TiO_2 surface and strengthen the coupling interaction, so the electron injection efficiency of sensitizers that adopted cyanoacrylic acid should be more excellent than sensitizers that adopted carboxylic acid. The Gibbs energy changes of electron injection of these sensitizers could reflect the electron injection efficiency. From the calculated results shown in Table

dx.doi.org/10.1021/jp2109829 | J. Phys. Chem. C 2012, 116, 9166−9179

4, one could get that the values of ΔG_{inject} are −1.6801, −1.6787, −1.6142, and −1.3974 for ZnBPP-PMCN, ZnBPP-PECN, ZnBPP-PE1, and ZnBPP-PMC1, respectively. These values are so close in energy that the probable error might flip the order. To confirm the reliability of the evaluation of the Gibbs energy change of electron injection, the driving forces were also calculated. The corresponding values of driving forces for these four sensitizers are 0.7101, 0.6695, 0.6128, and 0.4368, giving the same order as the Gibbs energy changes. From the schematic energy levels of porphyrins (as shown in Figure 6), all the calculated values of $E_{OX(dye^*)}$ of the four sensitizers are located above the CB (−0.44 V vs NHE) of TiO_2, indicating the electron injection process should be energetically favorable from the excited state of the dyes to the conduction band (CB) of TiO_2. What the excited-state oxidized potentials deliver is substantially the same as ΔG_{inject} and driving force. The electron injection efficiencies fulfilled the sequence of ZnBPP-PMCN > ZnBPP-PECN > ZnBPP-PE1 > ZnBPP-PMC1, which accords with our desired and discussed results.

It is known that the electron recombination process has strong distance dependence. The longer distance between the dye and TiO_2 surface could exhibit better performance due to a slower charge recombination rate.[12,29] The difference in linker length gives the distances of 14.87, 14.37, 12.30, and 12.30 Å between the ZnBPP center and the oxygen atom in the anchor group binding to the $Ti_{16}O_{32}$ surface for ZnBPP-PMCN, ZnBPP-PECN, ZnBPP-PM1, and ZnBPP-PE1, respectively. The orientation of sensitizer on the surface (shown in Supporting Information) is rather vertically arranged with the ZnBPP group pointing out from the surface. The D−B−A molecules with the cyanoacrylic acid anchoring group have longer distance between the light-harvesting centers and the TiO_2 surfaces, which could obtain relatively slower recombination rates for ZnBPP-PECN and ZnBPP-PMCN dyes, further enhancing charge collection efficiency. In addition, the evident anodic shifts of oxidized potentials of ZnBPP-PMCN and ZnBPP-PMC1 are more advantageous to improve the φ_{CC} than ZnBPP-PECN and ZnBPP-PE1 by avoiding the charge recombination, which can be accomplished through rapid regeneration of the sensitizers by a redox couple in a liquid electrolyte, such as the iodide/triiodide electrolyte. Besides, the introduction of pyrimidine may increase the energy barrier for electron recombination and facilitate the unidirectional electron injection due to the difference of coupling interaction. The coupling strength difference is advantageous for the electron separation, hindering the electron recombination.[31]

4. CONCLUSION

We have presented a computational investigation on the electronic structures and spectral properties of several novel designed porphyrin sensitizers, namely, ZnBPP-PECN, ZnBPP-PMC1, and ZnBPP-PMCN. For comparison, a series of zinc porphyrins with 1−3 π-conjugated phenylethylnyl (PE) units (labeled PE1−PE3) were also investigated in the present work. On the basis of the relevant preferred properties, for example, the optical absorption, the oxidized potential of ground and excited states, the light-harvesting efficiency, and the electron injection efficiency were calculated for providing electronic information about the roles electron-deficient pyrimidine and cyanoacrylic acid play in dominating the performances of sensitizers in the DSSC system. Briefly, we interpreted the reasons that sensitizer ZnBPP-PE1 obtains a low photo-to-electric conversion efficiency value of 2.7% in the DSSC system. The low efficiency is ascribed to the poor charge separation efficiency, limited regeneration of oxidized dye, and low light-harvesting efficiency in the longer wavelength range (Q band region), although a high light-harvesting efficiency was obtained in the *Soret* region. Structurally, the present calculations indicated that both the pyrimidine and the cyanoacrylic acid make significant adjustments to accommodate more outstanding photo-to-electric conversion efficiency, so we predicted that the ZnBPP-PMCN had the best photo-to-electric efficiency and was expected have the potential applicative perspective. The ZnBPP-PMCN obtained higher light-harvesting efficiency, more advantageous regeneration of oxidized dye, and more effective unidirectional electron movements relative to the other three and further obtained a higher conversion efficiency value. From the electron density difference plots of electron transitions, we can conclude that pyrimidine plays a key part in unidirectional electron movements, and the cyanoacrylic acid group could promote more electrons to move from the donor moiety to the acceptor group. Most importantly, the theoretical results revealed that the performance of photosensitizers in DSSCs not only relies on the spectral absorption intensity but also depends on the electron movement character related to the corresponding electron transition.

The present calculated results demonstrated a first attempt of providing a theoretical model for the introduction of electron-deficient pyrimidine bridged cyanoacrylic acid ending in porphyrin sensitizers. These results may provide structural guidelines for selecting the suitable π-spacer and anchor moiety to be used for further improved sensitizers in DSSC applications.

■ ASSOCIATED CONTENT

Supporting Information

Orbital energy levels, some important parameters including $\Delta G_{(aq)}$, E_{redox}, $E_{\lambda max}$, f, $E_{OX(dye)}$, $E_{OX(dye^*)}$, $\Delta G_{unrelax}$, D, and LHE of ZnBPP-PE*n* porphyrin sensitizers, electron density difference plots of surface complexes, the optimized molecule structures of surface complexes for bidentate adsorption on the $Ti_{16}O_{32}$ cluster of porphyrins sensitizers, and so on. This material is available free of charge via the Internet at http://pubs.acs.org.

■ AUTHOR INFORMATION

Corresponding Author

*E-mail: herx@swu.edu.cn; cyzhu@mail.nctu.edu.tw.

Notes

The authors declare no competing financial interest.

■ ACKNOWLEDGMENTS

We acknowledge generous financial support from Natural Science Foundation of China (20803059, 21173169) and Chongqing Municipal Natural Science Foundation (2009BB6002). C. Zhu would like to thank National Science Council of the Republic of China under grant no. 97-2113-M-009-010-MY3 for support.

■ REFERENCES

(1) (a) Service, R. F. *Science* **2005**, *309*, 548−541. (b) Potocnik, J. *Science* **2007**, *315*, 810−811.

(2) Schiermeier, Q.; Tollefson, J.; Scully, T.; Witze, A.; Morton, O. *Nature* **2008**, *454*, 816−823.

(3) (a) O'Regan, B.; Grätzel, M. *Nature* **1991**, *353*, 737−740. (b) Nazeeruddin, M. K.; Kay, A.; Rodicio, I.; Humphry-Baker, R.;

Mueller, E.; Liska, P.; Vlachopoulos, N.; Grätzel, M. *J. Am. Chem. Soc.* **1993**, *115*, 6382−6390. (c) Nazeeruddin, M. K.; Pechy, P.; Renouard, T.; Zakeeruddin, S. M.; Humphry-Baker, R.; Comte, P.; Liska, P.; Cevey, L.; Costa, E.; Shklover, V.; et al. *J. Am. Chem. Soc.* **2001**, *123*, 1613−1624.

(4) (a) Gao, F.; Wang, Y.; Shi, D.; Zhang, J.; Wang, M.; Jing, X.; Humphry-Baker, R.; Wang, P.; Zakeeruddin, S. M; Grätzel, M. *J. Am. Chem. Soc.* **2008**, *130*, 10720−10728. (b) Cao, Y.; Bai, Y.; Yu, Q.; Cheng, Y.; Liu, S.; Shi, D.; Cao, F.; Wang, P. *J. Phys. Chem. C* **2009**, *113*, 6290−6297.

(5) (a) Ito, S.; Nazeeruddin, M. K.; Liska, P.; Comte, P.; Charvet, R.; Pechy, P.; Jirousek, M.; Kay, A.; Zakeeruddin, S. M.; Grätzel, M.; et al. *Prog. Photovolt* **2006**, *14* (7), 589−601. (b) Kroon, J. M.; Bakker, N. J.; Smit, H. J. P.; Liska, P.; Thampi, K. R.; Wang, P.; Zakeeruddin, S. M.; Grätzel, M.; Hinsch, A.; Hore, S. *Prog. Photovoltaics* **2007**, *15* (1), 1−18. (c) Green, M. A.; Emery, K.; King, D. L.; Hishikawa, Y.; Warta, W. *Prog. Photovoltaics* **2007**, *15* (1), 35−40.

(6) Hagfeldt, A.; Boschloo, G.; Sun, L. C.; Kloo, L.; Pettersson, H. *Chem. Rev.* **2010**, *110*, 6595−6663.

(7) (a) Kay, A.; Grätzel, M. *J. Phys. Chem.* **1993**, *97*, 6272−6277. (b) Ishida, M.; Park, S. W.; Hwang, D.; Koo, Y. B.; Sessler, J. L.; Kim, D. Y.; Kim, D. *J. Phys. Chem. C* **2011**, *115*, 19343−19354.

(8) (a) Cherian, S.; Wamser, C. C. *J. Phys. Chem. B* **2000**, *104*, 3624−3629. (b) T Koehorst, R. B. M.; Boschloo, G. K.; Savenije, T. J.; Goossens, A.; Schaafsma, T. J. *J. Phys. Chem. B* **2000**, *104*, 2371−2377. (c) Lammi, R. K.; Richard, W. W.; Arounaguiry, A.; James, R. D.; David, F. B.; Dewey, H.; Jonathan, S. L. *J. Phys. Chem. B* **2001**, *105* (22), 5341−5352. (d) Jasieniak, J.; Johnston, M.; Waclawik, E. R. *J. Phys. Chem. B* **2004**, *108*, 12962−12971. (e) Balanay, M. P.; Dipaling, C. V. P.; Lee, S. H.; Kim, D. H.; Lee, K. H. *Sol. Energy Mater. Sol. Cells* **2007**, *91*, 1775−1781.

(9) (a) Tachibana, Y.; Haque, S. A.; Mercer, I. P.; Durrant, J. R.; Klug, D. R. *J. Phys. Chem. B* **2000**, *104*, 1198−1205. (b) Fungo, F.; Otero, L. A.; Sereno, L.; Silber, J. J.; Durantini, E. N. *J. Mater. Chem.* **2000**, *10*, 645−650. (c) Fungo, F.; Otero, L.; Durantini, E. N.; Silber, J. J.; Sereno, L. E. *J. Phys. Chem. B* **2000**, *104*, 7644−7651. (d) Eu, S.; Hayashi, S.; Umeyama, T.; Oguro, A.; Kawasaki, M.; Kadota, N.; Matano, Y.; Imahori, H. J. *Phys. Chem. C* **2007**, *111* (8), 3528−3537.

(10) (a) Odobel, F.; Blart, E.; Lagrée, M.; Villieras, M.; Boujtita, H.; Murr, N. E.; Caramori, S.; Bignozzi, C. A. *J. Mater. Chem.* **2003**, *13*, 502−510. (b) Nazeeruddin, M. K.; Humphry-Baker, R.; Officer, D. L.; Campbell, W. M.; Burrell, A. K.; Grätzel, M. *Langmuir* **2004**, *20* (15), 6514−6517.

(11) (a) Eu, S.; Hayashi, S.; Umeyama, T.; Matano, Y.; Araki, Y.; Imahori, H. *J. Phys. Chem. C* **2008**, *112* (11), 4396−4405. (b) Hayashi, S.; Tanaka, M.; Hayashi, H.; Eu, S.; Umeyama, T.; Matano, Y.; Araki, Y.; Imahori, H. *J. Phys. Chem. C* **2008**, *112* (39), 15576−15585.

(12) Park, J. K.; Lee, H. R.; Chen, J. P.; Shinokubo, H.; Osuka, A.; Kim, D. H. *J. Phys. Chem. C* **2008**, *112* (42), 16691−16699.

(13) (a) Lin, C.-Y.; Lo, C.-F.; Luo, L.-Y.; Lu, H.-P.; Hung, C.-S.; Diau, E. W.-G. *J. Phys. Chem. C* **2009**, *113*, 755−764. (b) Liu, Y.-J.; Na, X.; Feng, X.-M.; Shen, P.; Zhou, W.-P.; Weng, C.; Zhao, B.; Tan, S.-T. *Chem. Commun.* **2009**, 2499−2501. (c) Wu, S.-L.; Lu, H.-P.; Yu, H.-T.; Chuang, S.-H.; Chiu, C.-L.; Lee, C.-W.; Diau, E. W.-G.; Yeh, C.-Y. *Energy Environ. Sci.* **2010**, *3*, 949−955. (d) Lo, C.-F.; Hsu, S.-J.; Wang, C.-L.; Cheng, Y.-H.; Lu, H.-P.; Diau, E. W.-G.; Lin, C.-Y. *J. Phys. Chem. C* **2010**, *114*, 12018−12023.

(14) (a) Choi, H.; Paek, S.; Song, K.; Kang, M.-S.; Ko, J. *Bull. Korean Chem. Soc* **2010**, *31*, 125−132. (b) Li, Y.-T.; Chen, C.-L.; Hsu, Y.-Y.; Hsu, H.-C.; Chi, Y.; Chen, B.-S.; Liu, W.-H.; Lai, C.-H.; Lin, T.-Y.; Chou., P.-T. *Tetrahedron* **2010**, *66*, 4223−4229. (c) Chen, C.-H.; Hsu, Y.-C.; Chou, H.-H.; Thomas, K. R. J.; Lin, J. T.; Hsu, C.-P. *Chem.—Eur. J.* **2010**, *16*, 3184−3193. (d) Lin, L.-Y.; Tsai, C.-H.; Wong, K.-T.; Huang, T.-W.; Wu, C.-C.; Chou, S.-H.; Lin, F.; Chen, S.-H.; Tsai, A.-I. *J. Mater. Chem.* **2011**, *21*, 5950−5958.

(15) (a) Asbury, J. B.; Anderson, N. A.; Hao, E. C.; Ai, X.; Lian, T. Q. *J. Phys. Chem. B* **2003**, *107*, 7376−7386. (b) Hara, K.; Wang, Z. -S.; Sato, T.; Furube, A.; Katoh, R.; Sugihara, H.; Dan-Oh, Y.; Kasada, C.; Shinpo, A.; Suga, S. *J. Phys. Chem. B* **2005**, *109*, 15476−15482.

(16) (a) Becke, A. D. *J. Chem. Phys.* **1993**, *98*, 5648−5652. (b) Stratmann, R. E.; Scuseria, G. E.; Frisch, M. J. *J. Chem. Phys.* **1998**, *109*, 8218−8224. (c) Bauernschmitt, R.; Ahlrichs, R. *Chem. Phys. Lett.* **1996**, *256*, 454−464. (d) Casida, M. E.; Jamorski, C.; Casida, K. C.; Salahub, D. R. *J. Chem. Phys.* **1998**, *108*, 4439−4449.

(17) Lu, T. *Multiwfn*, version 2.1; http://multiwfn.codeplex.com/.

(18) (a) Casida, M. E.; Jamorski, C.; Casida, K. C.; Salahub, D. R. *J. Chem. Phys.* **1998**, *108*, 4439−4450. (b) Rosa, A.; Ricciardi, G.; Baerends, E. J.; van Gisbergen, S. J. A. *J. Phys. Chem. A* **2001**, *105*, 3311−3327. (c) Cramer, C. J. *Essentials of Computational Chemistry-Theories and Models*; John Wiley & Sons: Ltd.: New York, 2002; pp 252−253.

(19) (a) Fantacci, S.; De Angelis, F.; Selloni, A. *J. Am. Chem. Soc.* **2003**, *125*, 4381−4387. (b) De Angelis, F.; Fantacci, S.; Selloni, A. *Chem. Phys. Lett.* **2004**, *389*, 204−208. (c) Persson, P.; Maria, J. L. *J. Phys. Chem. B* **2005**, *109*, 11918−11924. (d) Muscat, J.; Wander, A.; Harrison, N. M. *Chem. Phys. Lett.* **2000**, *342*, 397−401. (e) Persson, P.; Gebhardt, J. C. M.; Lunell, S. *J. Phys. Chem. B* **2003**, *107*, 3336−3339. (f) De Angelis, F.; Tilocca, A.; Selloni, A. *J. Am. Chem. Soc.* **2004**, *126*, 15024−15025.

(20) Frisch, M. J.; Trucks, G. W.; Schlegel, H. B.; Scuseria, G. E.; Robb, M. A.; Cheeseman, J. R.; Scalmani, G.; Barone, V.; Mennucci, B.; Petersson, G. A.; et al. *Gaussian 09*, revision A.01; Gaussian, Inc.: Wallingford, CT, 2009.

(21) (a) Nilsing, M.; Persson, P.; Ojamae, L. *Chem. Phys. Lett.* **2005**, *415*, 375−380. (b) Lanzafame, J. M.; Palese, S.; Wang, D.; Miller, R. J. D.; Muenter, A. A. *J. Phys. Chem.* **1994**, *98*, 11020−11033.

(22) (a) Wiberg, J.; Guo, L.-J; Pettersson, K.; Nilsson, D.; Ljungdahl, T.; Mårtensson, J.; Albinsson, B. *J. Am. Chem. Soc.* **2007**, *129*, 155−163. (b) Wang, Q.; Campbell, W. M.; Bonfantani, E. E.; Jolley, K. W.; Officer, D. L.; Walsh, P. J.; Gordon, K.; Humphry-Baker, R.; Nazeeruddin, M. K.; Grätzel, M. *J. Phys. Chem. B* **2005**, *109*, 15397−15409. (c) Pettersson, K.; Wiberg, J.; Ljungdahl, T.; Mårtensson, J.; Albinsson, B. *J. Phys. Chem. A* **2006**, *110*, 319−326. (d) Kilså, K.; Kajanus, J.; Macpherson, A. N.; Mårtensson, J.; Albinsson, B. *J. Am. Chem. Soc.* **2001**, *123*, 3069−3080.

(23) Ooyama, Y.; Shimada, Y.; Kagawa, Y.; Yamada, Y.; Imae, I.; Komaguchi, K.; Harima, Y. *Tetrahedron Lett.* **2007**, *48*, 9167−9170.

(24) Wang, J.; Bai, F.-Q.; Xia, B.-H.; Feng, L.; Zhang, H.-X.; Pan, Q.-J. *Phys. Chem. Chem. Phys.* **2011**, *13*, 2206−2213.

(25) Preat, J.; Michaux, C.; Jacquemin, D.; Perpete, E. A. *J. Phys. Chem. C* **2009**, *113*, 16821−16833.

(26) Ooyama, Y.; Shimada, Y.; Kagawa, Y.; Yamada, Y.; Imae, I.; Komaguchi, K.; Harima, Y. *Tetrahedron Lett.* **2007**, *48*, 9167−9170.

(27) Katoh, R.; Furube, A.; Yoshihara, T.; Hara, K.; Fujihashi, G.; Takano, S.; Murata, S.; Hironori Arakawa, H.; Tachiya, M. *J. Phys. Chem. B* **2004**, *108* (15), 4818−4822.

(28) Cave, R. J. *J. Phys. Chem. A* **2002**, *106*, 9294−9305.

(29) (a) Rochford, J.; Chu, D.; Hagfeldt, A.; Galoppini, E. *J. Am. Chem. Soc.* **2007**, *129* (15), 4655−4665. (b) Schlichthorl, G.; Park, N. G.; Frank, A. J. *J. Phys. Chem. B* **1999**, *103*, 782−791.

(30) Alebbi, M.; Bignozzi, C. A.; Heimer, T. A.; Hasselmann, G. M.; Meyer, G. J. *J. Phys. Chem. B* **1998**, *102* (39), 7577−7581.

(31) Nalwa, H. S. *Handbook of Advanced Electronic and Photonic Materials and Devices*; Academic, Elsevier: San Diego, 2001; pp 2001−35